Effects of Compressive Stress on Glioblastoma Cells

THESIS

Presented in Partial Fulfillment of the Requirements for the Honors Research Distinction in the Undergraduate School of The Ohio State University

By

Eileen Elliott

Undergraduate Honors Program in Chemical and Biomolecular EngineeringChemical and Biomolecular Engineering

The Ohio State University

2017

DissertationDissertation Committee:

Jessica Winter Advisor, David Wood

Abstract

The application of engineering principles and technologies to biological systems has enabled the advent of new healthcare strategies. This research is focused on understanding the effects of compression on the migration of brain tumor cells in vitro and to understand the molecular underpinnings regarding this change. Compression in the brain arises as a result of the barrier formed by the cranium. As intracranial pressure increases, because of head injury or tumor growth, compression will increase. Untreated compression in the brain can lead to the destruction of brain tissue and even death. Previous studies have shown that increasing compression on breast cancer cells leads to an increase in migration. The increase in migration of cancer cells in comparison to somatic cells may explain a portion of the invasive nature of cancer cells. We examined the effects of different compressive forces applied to cells and how force affects migration using three types of glioblastoma brain cancer cells.

To assess cell migration and proliferation, a traditional wound healing assay was employed, as well as a 3D single cell migration assay that evaluates the multi-

directionality of cell migration. To complete the 3D migration assay, a hydrogel was engineered to have the specific viscosity and elasticity that mimics the environment of the brain. We found that increasing the pressure (compression) above 23 Pa causes a decrease in the migration of the glioblastoma cells. Additionally, to determine how the compressive stress affects the cells, a single cell morphology experiment was completed, which indicated that compressive stress decreases cell area and ferret length. This conclusion contrasts with the previous research model that described the link between compressive stress and migration for breast cancer cells. Our long-term objective from this research is to elucidate the effect of compressive solid stress on glioblastoma cell migration to identify possible drug interventions and to translate this finding to the clinical treatment.

Acknowledgments

I would like to thank Mark Calhoun and Dr. Jessica Winter for being fantastic mentors, and supporting me along the way, as well as my parents for helping me read through my thesis.

Vita

June 2012 .....Walsh Jesuit High School

2012 to present .....B.S. Chemical Engineering, Department of Chemical and Biomolecular Engineering, The Ohio State University

Fields of Study

Major Field: Chemical and Biomolecular EngineeringChemical and Biomolecular Engineering

Table of Contents

Effects of Compressive Stress on Glioblastoma Cells 1

Abstract ii

Acknowledgments iv

Vita v

Fields of Study v

Table of Contents vi

List of Tables ix

List of Figures xi

Introduction 14

Significance 14

Literature Review 15

Thesis Overview 17

Specific Aim 1: Characterization of cell line migration under no stress. 18

Specific Aim 2: Compare the wound healing assays of cells that undergo mechanical stress to control glioblastoma cells as well as determine a mechanism to explain this increase in migration. 19

Specific Aim 3: Create a hydrogel with the same biophysical properties of the brain to study the 3D effects of compression on the cells. 24

Results and Discussion 26

Specific Aim 1: Characterization of cell line migration under no stress. 26

Specific Aim 2: Compare the wound healing assays of cells that undergo mechanical stress to control glioblastoma cells as well as determine a mechanism to explain this increase in migration. 28

Specific Aim 3: Create a hydrogel with the same biophysical properties of the brain to study the 3D effects of compression on the cells. 32

Conclusion 36

References 39

Appendix A: Specific Aim 1 Raw Data 41

Appendix B: Specific Aim 2 Raw Data 53

List of Tables

Table 1: Preliminary Results of Hydrogel Testing using Non-Thiolated Collagen..... 33

Table 2: Preliminary Results of Hydrogel using Thiolated Collagen..... 34

Table 3: LN229 Single Cell Migration Raw Data 41

Table 4: U87 Single Cell Migration Raw Data..... 42

Table 5: U251 Single Cell Migration Raw Data..... 44

Table 6: U87 (Edu Test) Proliferation Characterization Raw Data..... 48

Table 7: U251 (Edu Test) Proliferation Characterization Raw Data..... 50

Table 8: LN229 (Edu Test) Proliferation Characterization Raw Data 52

Table 9: LN229 Wound Healing Assay Raw Data..... 53

Table 10: U251 Compressive Stress Wound Healing Assay Raw Data..... 55

Table 11: LN229 Single Cell Morphology Data..... 57

Table 12: U251 Single Cell Morphology Data..... 58

List of Figures

Figure 1: Normal Mammary (MCF10A) and Cancer (67NR) Cells Closing a Wound in the Wound Healing Assay (16 h) [6]. 16

Figure 2: 1D Wound Healing Assay with Ibidi Chamber..... 20

Figure 3: Schematic of Experimental Setup for Effects of Compressive Stress using 1D Wound Healing Assay 21

Figure 4: Jain's Proposed Model of compression-modulated leader-cell formation and coordinated migration. (A) Cells seeded at the corners and edges of square islands have different extents of free perimeter, which affect actomyosin-driven intracellular stress. (B) Uncompressed cultures. (C) The resulting change in force balance within the cell likely causes their phenotypic change into "leader" cells. (D) Culture is compressed, all cells around the periphery of the island are deformed, or extruded, against the substrate, into the empty space. (E) Hence, all cells around the periphery of the square pattern can become leader cells. [2] 22

Figure 5: Schematic of Compressive Solid Stress Model. GB cells are cultured in a collagen I gel with an agarose cushion on top of the gel to reduce edge effects; Aluminum discs applied varying levels of compressive force..... 25

Figure 6: Characterization of Cell Line (A) Migration and (B) Proliferation under Normal Conditions. Star indicates $p < 0.05$ when compared to the U251 cell line..... 26

Figure 7: Characterization of compressive stress effects on migration for (A) LN229 cell line and (B) U251 cell line. Star indicated $p < 0.05$ when compared to control and crossbar indicates $p < 0.05$ when compared to agar control. 28

Figure 8: LN229 Cell Line under CellTracker Green Fluorescence under Different Compressive Stress (A) Control, (B) Agar Control (C) 23 Pa Compressive Stress (D) 47 Pa Compressive Stress 30

Figure 9: Characterization of Compressive Effects on Morphology (Cell Area) for (A) the LN229 cell line and (B) the U251 cell line. Star indicates $p<0.05$ when compared to the control; crossbar indicates $p<0.05$ when compared to the agar control; red star indicates $p< 0.05$ when compared to 23 Pa. 30

Figure 10: Characterization of compressive stress effects on ferret length for the (A) LN229 cell line and the (B) U251 cell line. Star indicates $p<0.05$ when compared to the control; crossbar indicates $p<0.05$ when compared to the agar control. Red star indicates significant difference of $p<0.05$ when compared to 23 Pa. 31

Introduction

Significance

Glioblastoma (GBM) is an invariably devastating cancer resulting in an overall survival of 15 months after diagnosis [1]. Furthermore, GBM is a highly malignant type of brain tumor that makes up 15.4% of the primary brain tumors that occur [3]. GBM is a uniquely aggressive cancer because of several characteristics, including inherent resistance to conventional therapy, limited capacity of the brain to repair itself, and migration of malignant cells into adjacent brain tissue. Furthermore, GBMs are composed of a wide variety of cell types, which are supported by a large network of blood vessels within the brain, limiting treatment options [3]. Because of these limitations, the median two-year survival rate is 30%. Therefore, a better understanding of what makes GBM such an aggressive cancer is necessary to create better treatment options.

Currently, the treatments for GBM include concurrent radiation, chemotherapy, and surgical resection. Both treatments function by damaging deoxyribonucleic acid (DNA). Nevertheless, GBM invariably reoccurs, leading to most patients developing resistance to such therapies and ultimately succumbing to the disease. Instead of focusing on damaging the DNA, the long-term goal of this research is focused on increasing

understanding of how GBM cell migration is related to specific phenotype expression. Through understanding the relationship between phenotype changes resulting from mechanical stress that occurs during tumor growth and migration, new methods to inhibit these phenotypes and treat the GBM cells can be identified.

Literature Review

During progression, the tumor induces specific physical forces in the microenvironment that inevitably affect treatment efficacy. It has been determined that specific cancer cells will increase in their growth rate in response to mechanical stresses. As the tumor grows, the mechanical stress increases because of the cranium creating a barrier. Therefore, the mechanical stress will cause GBM cell phenotype to change and increase the migration and proliferation of some cells [2].

The compressive forces resulting from tumor growth provide solid tissue stresses (STS) estimated at ~ 10 to 100 mmHg [4]. STS can lead to increased interstitial fluid pressure (IFP) and can lead to a cranial pressure 10 X that of normal brain tissue, halting interstitial fluid flow (IFF) [5]. Since IFF occurs along the white matter tracts within the brain, this is thought to enhance the migration of the GBM cells, since these cells are known to migrate alone Scherer's structures, such as white matter tracts. Furthermore, in a previous study observing the effects of mechanical stress on cancer cells, specifically carcinoma cells, it was found that as the mechanical stresses increase, the ‘leader’ phenotype becomes more prevalent, increasing the occurrence of leader cells [5]. Leader

cells are defined as those cells at the wound margin that extend protrusions into the denuded area [5].

Therefore, as more leader cells appear, more migration occurs (Figure 1). From Figure 1, it is apparent that the compressed cancer cells exhibited directional alignment and faster migration, whereas the control cells displayed suppressed migration [6]. Because of this previous research, we hypothesized that as the mechanical stress increases on the glioblastoma cells, the leader phenotype, and therefore migration, would increase. However, in this previous research, this behavior was theorized to result from the cancer cells being compressed and therefore migrating into the open space to relieve this pressure [6]. In this research, we also desired to understand a more specific mechanism for observed changes in migration.

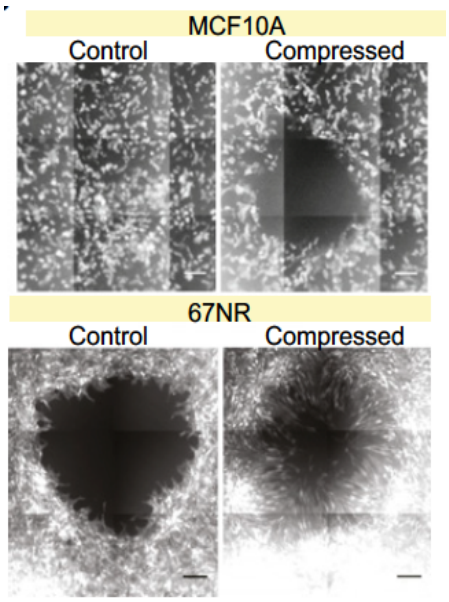

Figure 1: Normal Mammary (MCF10A) and Cancer (67NR) Cells Closing a Wound in the Wound Healing Assay (16 h) [6].

Thesis Overview

There are no current effective treatments to treat glioblastoma tumors that occur in the brain. However, with the investigation of the relationship between phenotype changes because of mechanical stress and migration, additional treatments to prevent the appearance of the migratory phenotype may result.

Our long-term objective was to identify the glioblastoma phenotype associated with increased migration under stress. Our short-term objective was to create a mechanical stress experiment to observe cell phenotype changes and migration in both 1D and 3D. In completing this research, three glioblastoma cell lines, LN229, U87, and U251, were studied. The goals of this research were divided into three specific aims.

Specific Aim 1: Characterization of cell line migration behavior under no stress, control conditions.

Specific Aim 2: Determine if compressive stress increases the migration of glioblastoma cells and if so what mechanism explains this.

Specific Aim 3: Create a hydrogel with that mimics biophysical properties of the brain to study the 3D effects of compression on the cells.

Research Methodology

Specific Aim 1: Characterization of cell line migration under no stress.

Rationale: In order to understand how the cells change under compressive stress, the migration of cells under normal conditions must be characterized for comparison. To do this, migration of three cell lines was characterized using a single cell migration experiment. Multiple cell lines are necessary since the GBM's resistance to conventional therapies is because GBM is made up of multiple cell types supported by a matrix of blood vessels. The cell lines we chose to study were the U87 cell line, the LN229 cell line, and the U251 cell line. The three cell lines were chosen since they are the most commonly used with U87 having more than 1900 PubMed citations [9]. This allowed for us to have higher confidence in our results and any conclusions we draw. In addition, they were chosen for their different natures, specifically with U87 exhibit a higher capacity for migration and invasion when compared to other cell lines [10].

For single cell migration, 10,000 cells were stained CellTracker Green and placed upon a Transwell filter to allow for nutrients to flow to the cells while the movement of cells through the filter was prevented. Transwell filters are permeable supports that allow for

the cells to adhere to them to better study cell lines *in vitro* by limiting disturbances to the cells. These cells were allowed to adhere for 24 hours. Following this, time lapse fluorescence imaging of the cells for 18 hours was completed. Using time lapse, the migration of each cell imaged over 18 hours was characterized.

In addition to characterizing the migration of each cell line, the proliferation of each cell line was also characterized. This was done by staining DNA using an Alexa-Fluor fluorescence assay using the ThermoFisher Click-It Plus Imaging Kit [7]. Using this kit, cells were stained with two different stains. One stain identified all cells present, whereas the other stain identified cells that had newly synthesized DNA. The cells were imaged using two different fluorescence filters, FITC and DAPI, to visualize the different stains. The number of cells that appeared under FITC, the DNA stain, was compared to the number of cells that appeared under the DAPI fluorescence, the nuclear stain.

Specific Aim 2: Determine if compressive stress increases the migration of GBM cells and if so what mechanism explains this.

Rationale: To observe whether the leader phenotype occurs more frequently at higher pressures a wound healing assay was used. A 1D wound healing assay was used on cells from the uncompressed (0 Pa) condition and compared to the wound healing assays of the other compressions up to 165 Pa. The compression values most frequently tested were 13 Pa $\pm$ 0.55 Pa, 23 Pa $\pm$ 0.39 Pa, and 47 Pa $\pm$ 0.31 Pa. To complete the assay, each cell line

was stained and placed in an Ibidi chamber. An Ibidi chamber is a chamber that patterns cell cultures into specific shapes in 1D cultures. The cells are placed in two separating compartments, 200,000 cells in each compartment, and left to adhere to the plate for six hours, thus creating a gap between cell populations. Two time points of this setup were evaluated, at t=0, and t=18 hours. The migration was then quantified by the area the cells covered after 18 hours. An example of such a setup can be seen in Figure 2.

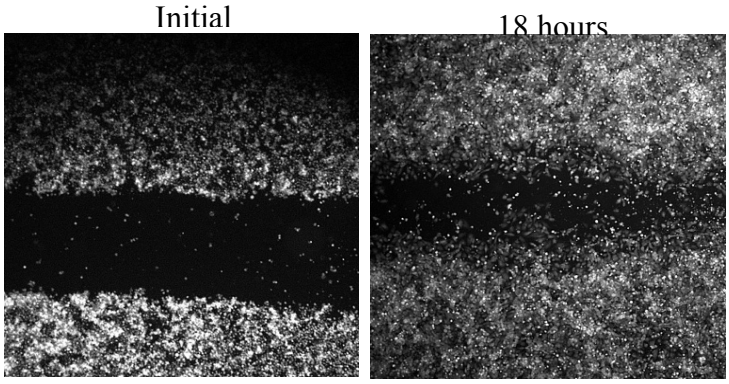

Figure 2: 1D Wound Healing Assay with Ibidi Chamber

To characterize the percent wound healing, the area of the space between the compartments was measured for both time points using NIH ImageJ image analysis software. The wound healing percent was then calculated using Equation 1.

$$\%\, Wound\ Healing = \frac{Area_{initial} - Area_{Final}}{Area_{initial}}$$ Equation 1

Using the Ibidi chamber protocol, a compressive stress model was developed to test how a variety of mechanical stresses affect the cells. The experimental setup design can be seen in Figure 3. An agarose hydrogel cushion was placed on top of the cells, as well as

aluminum discs to create compression. In addition to aluminum discs, a vinyl disc was used to achieve the lowest compression, of 13 Pa. Two controls were used in each experiment, a control with nothing on top of the cells, as well as an agar control in which the agarose cushion was placed upon the cells.

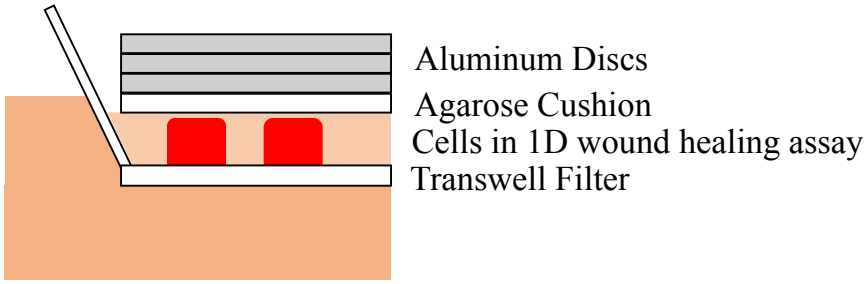

Figure 3: Schematic of Experimental Setup for Effects of Compressive Stress using 1D Wound Healing Assay

This setup was used for all three cell lines. The migration of the cells was be recorded by taking pictures with a microscope at two time points, 0 and 18 hours. To characterize the migration, the percent of wound healing from Equation 1.

After the effects of compression on migration were determined, it was desired to understand how the effects of compression caused the morphology of the cells to change. This was also evaluated to attempt to determine a possible mechanism for interactions between compressive stress and migration. Building upon previous research done by Jain et al., (6), it was expected that migration would increase as cells attempted to find more room for growth and to relieve compressive forces. In this proposed mechanism,

Figure 4, Jain describes that the increase in the invasive phenotype results from an increase in the leader phenotype, the phenotype for cells that first migrate leading other cells to follow. This increase is results from the compressive force causing the cells to flatten and extrude outwards, therefore increasing migration. If the mechanism proposed by Jain et al. is correct, we would expect for compressive stress in our system to increase the area covered by cells compared to the controls.

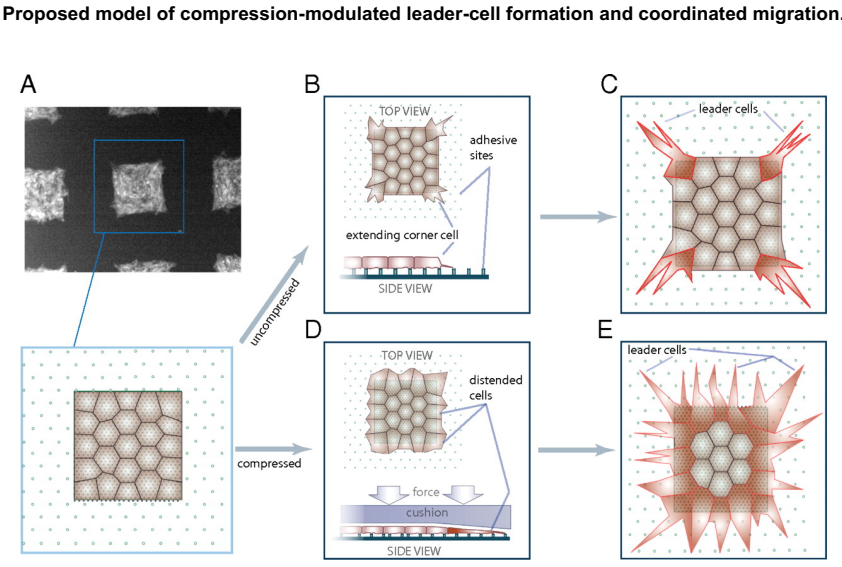

Figure 4: Jain's Proposed Model of compression-modulated leader-cell formation and coordinated migration. (A) Cells seeded at the corners and edges of square islands have different extents of free perimeter, which affect actomyosin-driven intracellular stress. (B) Uncompressed cultures. (C) The resulting change in force balance within the cell likely causes their phenotypic change into "leader" cells. (D) Culture is compressed, all cells around the periphery of the island are deformed, or extruded, against the substrate, into the empty space. (E) Hence, all cells around the periphery of the square pattern can become leader cells. [2]

In our system, morphology was characterized by staining 10,000 cells and placing them on Transwell filters to adhere for 24 hours. Following adherence, the setup illustrated in

Figure 3 was used to evaluate two controls and the same cell lines at two pressures. All membranes were evaluated at t= 0 and after 18 hours. Subsequently, images of the cells were taken by placing a microscope slide on the bottom of the membrane to ensure higher image quality. The change in cell morphology was then characterized by determining the ferret length, as well as the area of each cell. The ferret length is the distance from the two outmost points in a single cell, whereas the area of the cell was determined by circling the shape of the cell and measuring the area. Both measurements were completed in ImageJ.

Once the effects of compression on the cells were determined, we attempted to identify the mechanism responsible for this response. This was done by completing a Western Blot, evaluating if compressive stress alters migration rate by focal adhesion kinase (FAK) signaling. This pathway was hypothesized to be involved in mechanically induced migration because FAK has been shown to have a strong role in controlling cell motility (8). The FAK signaling pathway, along with the myosin light chain-2 (MLC-2) signaling pathway, was studied. Actin was used as a control. The myosin light chain signaling pathway was also studied since it is used in migration as well as is upregulated in gliomas [11].

Specific Aim 3: Create a hydrogel with the same biophysical properties of the brain to study the 3D effects of compression on the cells.

Rationale: Previous research has indicated that 2D and 1D models do not adequately represent how glioblastoma cells react in-vivo. This is because these systems have been reported to exhibit markedly different responses to cytotoxic treatments than those observed in patients [12]. Therefore, to understand the relationship between compression and changes in GBM in their natural environment, a 3D migration assay was designed and implemented. This required the development of a hydrogel with the same mechanical properties as the brain to adequately represent the environment that the GBM cells experience. This was done by using an ESIBIO hydrogel kit and altering the concentrations of thiolated-HA, collagen, polyethylene glycol diacrylate (PEGDA) to achieve an elastic modulus of ~1.4 kPa. This elastic modulus was identified as targets through testing of a pig brain in our lab performed previously. The thiolated-HA was since it makes up the extracellular matrix, and is the most abundant matrix molecule in normal and cancer brain tissue. Collagen was used in our to model the matrix of blood vessels that supports the cells. The PEGDA was a cross-linker used to react with the HA and collagen to form the hydrogel matrix.

Using a parallel plate compression machine, stress-strain curves were collected, and the global modulus, elastic modulus, and viscosity were determined from these tests. The raw data and curves for hydrogel testing are provided in Appendix A. The ratios of HA,

collagen, and PEGDA were varied until a final elasticity of 1.4 kPa and viscosity of 116000 $N \cdot s \cdot m^{-2}$ were achieved.

Once a desired hydrogel was created, the effects of compression on the 3D morphology of the cells were determined. This was performed by placing 175k GBM cells per ml of hydrogel into a gel of ~1 mm in thickness. These specifications were used to be consistent with the Munn-Jain model [6]. These hydrogels were then allowed to culture for 24 hours. Following this, an agarose cushion and aluminum discs were added to create compression. A schematic demonstrating this setup can be seen in Figure 5. Two controls were used in each experiment, a control with nothing on top of the hydrogel and an agar control in which the agarose cushion was placed upon hydrogel. These were permitted to culture for 18 hours to see the effects of compression. Finally, images of the cells were taken using microscopy; and the ferret diameter and area of each cell in the images was recorded.

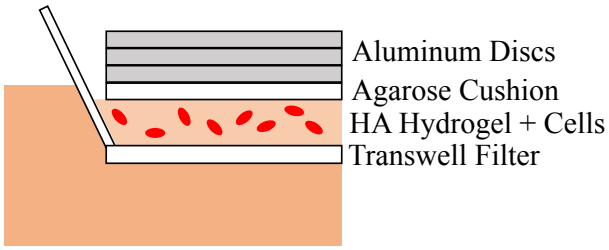

Figure 5: Schematic of Compressive Solid Stress Model. GB cells are cultured in a collagen I gel with an agarose cushion on top of the gel to reduce edge effects; Aluminum discs applied varying levels of compressive force

Results and Discussion

Specific Aim 1: Characterization of cell line migration under no stress.

Initially, the migration and proliferation of all three cell lines under normal conditions were determined. Migration behaviors of the three cell lines were compared using single cell migration models. Figure 6A shows results for the three cell lines, whereas raw data is found in Appendix A. In addition to the migration speed for each cell line, the proliferation speed was also compared, which can be seen in Figure 6B.

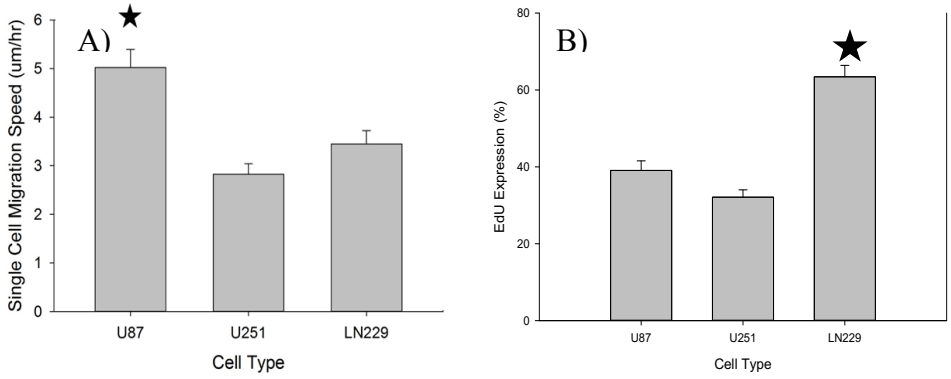

Figure 6: Characterization of Cell Line (A) Migration and (B) Proliferation under Normal Conditions. Star indicates $p < 0.05$ when compared to the U251 cell line

To analyze these results, both the lengths of migration as well as the distance from the starting point were considered. Using the length of the path traveled by the cell, and the total observation time, 18 hours, the single cell migration speed was determined. Using these results, it was determined that the U87 cell line was the more invasive cell line compared to the other cell lines studied. An ANOVA tukey test was completed and this indicated that the U87 cell line was significantly more invasive when compared to the U251 cell line, while the LN229 was more proliferative when compared to the U251 cell line. These results are consistent with previous research indicating the U87 was the most migratory cell line [10].

Figure 6 also illustrates that, whereas the U87 cell line had a higher migration speed, it had reduced proliferation compared to the LN229 line. Whereas the U87 cell line may be more invasive, the LN229 cell line is more proliferative cell line compared to the other cells. This shows that the LN229 cells line grows faster in comparison to the other cell lines. This also provides a baseline for cell migration and proliferation under normal conditions. In addition, it allows us to compare migration rates between cell lines to ensure such a comparison is consistent. For example, if the U251 cell line has lower migration under compressive stress than the U87, this could potentially be explained by its lower migration under normal conditions.

Specific Aim 2: Determine if compressive stress increases the migration of GBM cells and if so what mechanism explains this.

Due to possible contamination, the U87 cell line was unable to be characterized, and only the LN229 and U251 cell lines were observed. Initially, high amounts of compressive stress were tested to be consistent with previous research. These measurements were performed by placing stainless steel discs on top of the cells under an agar cushion. The initial pressures tested were 58 Pa to 165 Pa. These pressures decreased migration speeds. Therefore, lower pressures were evaluated. To achieve lower pressures, aluminum discs were used because of their lower weight, as well as vinyl discs, to achieve pressures of 11 Pa, 23 Pa, and 47 Pa. Figure 8 below illustrates the effect of compression on LN229 and U251 cell lines.

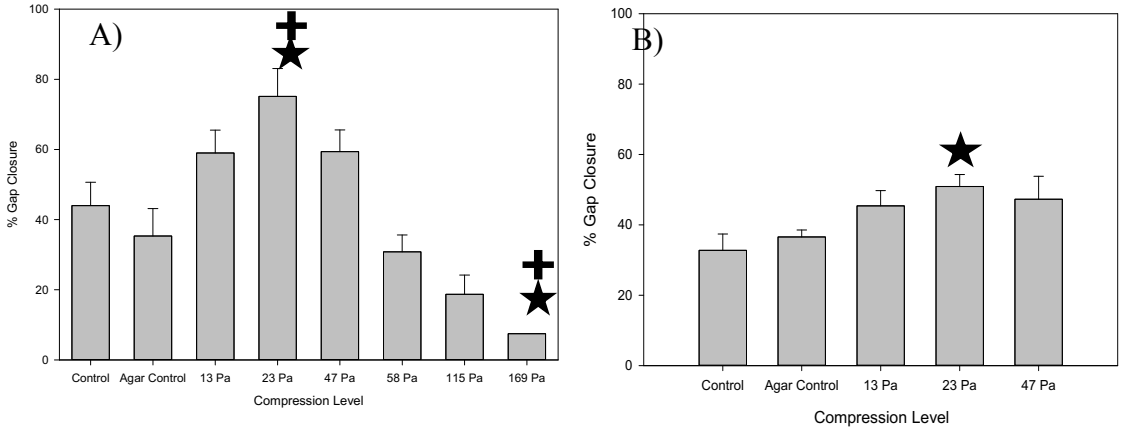

Figure 7: Characterization of compressive stress effects on migration for (A) LN229 cell line and (B) U251 cell line. Star indicated $p < 0.05$ when compared to control and crossbar indicates $p < 0.05$ when compared to agar control.

In Figure 7A, for L229 cells, the relationship between migration and compression yields a parabolic curve. This trend indicates that as compression increases, migration increases, up to a specific compression point, in this case 23 Pa. After this point, increasing compression causes a decrease in migration speed. This trend is consistent with previous research performed by Jain et. al (6). This indicates that, whereas migration initially increases under compression, high levels of compression can cause decreases in migration rates, perhaps resulting from too much stress. However, there was no apparent increase in cell death between increased compression experiments and the controls.

The U251 cell line displayed a similar trend to the LN229 cell line. However, there was a decrease in the amount of gap closure for each of the conditions in comparison to the LN229. This is consistent with the single cell migration data that indicated that the U251 cell line had a lower migration speed under normal conditions. This may also account for the less drastic effect of compressive stress on migration speed, as well as why the control has a lower gap closure than that of the LN229 line. It should be noted with the U251 cell line, whereas there was no significant difference between the agar control, 23 Pa, and 47 Pa conditions, there was a similar trend to the LN229 in which there was a significant difference.

To achieve a better understanding of cell responses under compressive stress, single cell morphologies were evaluated. Effects at pressures of 23 Pa and 47 Pa were evaluated to determine if changes in migration speeds were correlated to changes in the cell shape Imaged cells under increasing compression can be seen in Figure 8.

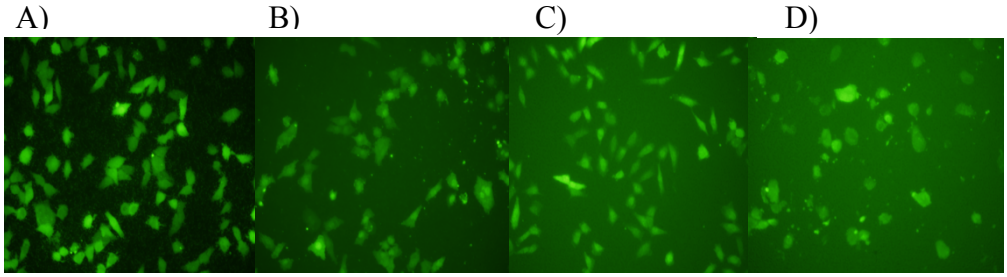

Figure 8: LN229 Cell Line under CellTracker Green Fluorescence under Different Compressive Stress (A) Control, (B) Agar Control (C) 23 Pa Compressive Stress (D) 47 Pa Compressive Stress

To quantify the results in Figure 8, the cell area and Ferret length of each cell were determined. Figure 9, illustrates the change in cell area between the different conditions of compressive stress for the LN229 cell line.

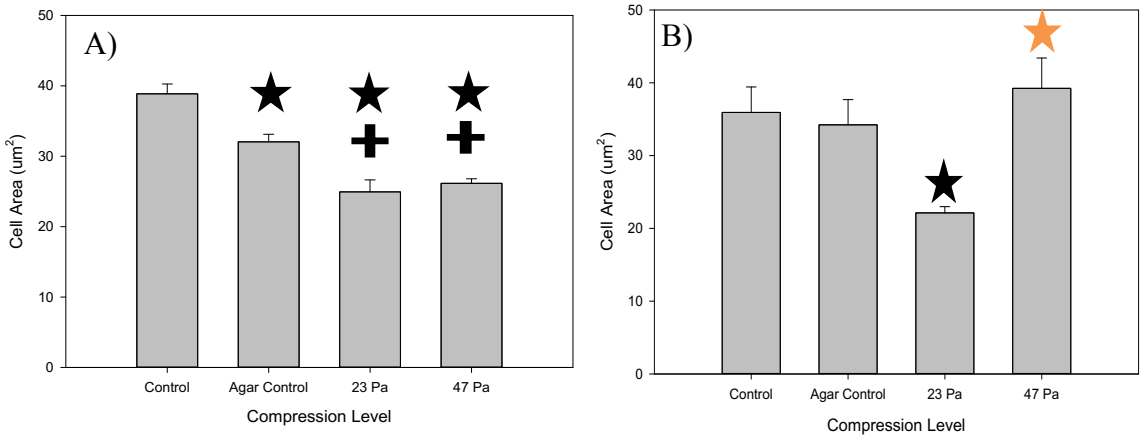

Figure 9: Characterization of Compressive Effects on Morphology (Cell Area) for (A) the LN229 cell line and (B) the U251 cell line. Star indicates $p<0.05$ when compared to the control; crossbar indicates $p<0.05$ when compared to the agar control; red star indicates $p< 0.05$ when compared to 23 Pa.

For the LN229 cell line, the 23 Pa, 47 Pa, and agar control were significantly different from the control. Additionally, the 23 Pa and 47 Pa compressions were significantly

different from the agar control. However, for the two experimental conditions (23 Pa and 47 Pa) in the LN229 cell line, there was no significant difference between the two. However, the two were both significantly different from the two controls. On the other hand, in the U251 line, there was an increase in the cell area in the 47 Pa compression sample compared to the 23 Pa sample. This may indicate that a decrease in cell area is correlated to an increase in migration. In addition to the cell area, the Ferret length was also compared which can be seen in Figure 10.

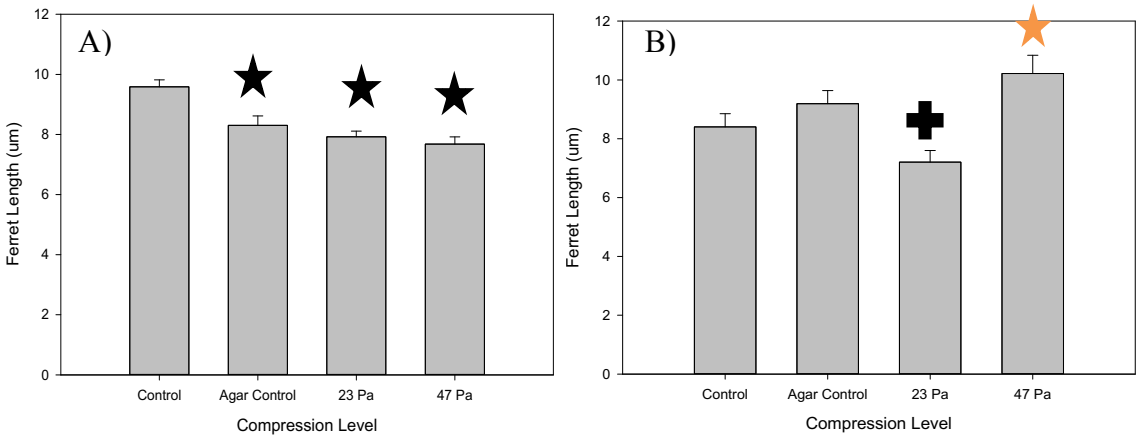

Figure 10: Characterization of compressive stress effects on ferret length for the (A) LN229 cell line and the (B) U251 cell line. Star indicates $p<0.05$ when compared to the control; crossbar indicates $p<0.05$ when compared to the agar control. Red star indicates significant difference of $p<0.05$ when compared to 23 Pa.

In the comparison of Ferret length between compressive stress conditions in the LN229 line, only the control was significantly different from the other three conditions. For the U251 cell line, only the 23 Pa was significantly different from the agar control and there was no significant difference between the control and the other conditions. This could

indicate that at this compressive stress the cells are becoming more circular and increasing their area but decreasing their maximum length. However, the U251 cell line's area increased as the compression increased past 23 Pa. Therefore, there is a desire to determine if this same trend occurs at higher compressions for the LN229 cell line.

These results contradict the proposed model described by Jain's group (8). Since we saw a decrease in cell area with increasing compressive force, cells were not expansively flattened by compressive force. Therefore, an alternative mechanism may be needed to describe the observed migration behaviors. To explore a possible mechanism, we are completing Western Blots to determine what, if any, signaling pathways may be involved in migration. However, these results were not conclusive at the time of this thesis.

Specific Aim 3: Create a hydrogel with the same biophysical properties of the brain to study the 3D effects of compression on the cells.

After the 2D wound healing assays and morphology tests were completed, it was desired to evaluate cell migration and compressive stress in 3D, using more physiological models. This required design and engineering of a hydrogel with the same biophysical properties of brain. This was achieved by varying ratios of thiol-modified hyaluronan (HA), pure-col, a type of collagen, and thiol-reactive PEGDA cross-linker to yield hydrogels of different stiffness. These ratios were altered to achieve an elasticity of 1.4 kPa and 116,000 N s m^{-2}. Table 1 shows the preliminary results of the hydrogels created.

Table 1: Preliminary Results of Hydrogel Testing using Non-Thiolated Collagen

	HA:Collagen:PEDGA:Media		
Sample Ratio	4:2:1:0.61	2:4:1:0.61	10:10:1:2
global modulus (kPa)	22.148	20.914	20.540
elastic modulus (kPa)	16.642	12.285	5.9742
tau	74.180	22.621	24.405
viscosity (kPa*s)	1046.6	280.07	145.72
R2 Stress Strain Curve	0.96375	0.95378	0.96835
R2 Stress relaxation Curve	0.59314	0.8742	0.71519

These results indicate that by increasing the ratios of HA and collagen to PEGDA, the elasticity decreases. However, these results demonstrate substantial variability that was determined to result from the use of a non-thiolated collagen. This variability is because the PEGDA increases the stiffness by covalently cross-linking thiol groups on the hyaluronic acid. Since the pure-col is not thiolated, PEGDA crosslinking does not influence collagen gelation. As a result, thiolated, denatured collagen, i.e., Glycosil, produced by ESI-Bio was used instead. Based on the results of the pure-col formulations, a similar 10:10:1:2 ratio of HA:Glycosil:PEGDA:Media as well as following the ESI-bio protocol of having a 2:2:1 ratio of HA:Glycosil:PEGDA and using the minimum of 100 μL of media were evaluated. The preliminary results of the hydrogel testing can be seen in Table 2.

Table 2: Preliminary Results of Hydrogel using Thiolated Collagen

	HA:Gelin-S:PEDGA:Media	
Sample Ratio	10:10:1:2	2:2:1:0.61
global modulus (kPa)	32.14	3.74
elastic modulus (kPa)	5.89	17.93
tau	20.91	3.55
viscosity (kPa*s)	133.44	53.12
R2 Stress Strain Curve	0.74	0.45
R2 Stress relaxation Curve	0.22	0.27

These results indicate that following the ESI-bio protocol leads to a higher elastic modulus than desired. Additionally, we were able to achieve a similar elastic modulus as before, with the non-thiolated collagen, indicating that this new collagen cause little change to the elasticity, but decreases variability. Additionally, from the results, the elastic modulus was able to be decreased by increasing the ratio of HA and Gelin-s to PEGDA, but diluting the PEGDA concentration by two in DI water also decreases the elastic modulus. Hydrogels using this method were created; however, because of their low elastic modulus, were not able to be removed from the gelation plate without damage. This limited ability to test the mechanical properties of the material. Therefore, we are currently attempting to engineer a better methodology to test this hydrogel without disturbing the hydrogel matrix. I have proposed a methodology to combat the issues seen during testing by placing a film in the well prior to placing the hydrogel within this well. This will allow us to remove the hydrogel from the well, during testing, without disturbing the hydrogel matrix by simply pulling the film out of the well with the hydrogel supported by the film. This approach will be employed in future work. Study of

the effects of compressive stress on 3D single cell migration will also form the subject of future work.

Conclusions

Glioblastoma (GBM) is an invariably devastating cancer because of its aggressiveness and low mean survival time. Because of this, there is a desire to develop new treatments for glioblastoma, besides the currently used methods of chemotherapy, radiation, and surgical resection. To develop new treatments, it is necessary to understand the invasive nature of GBM. To accomplish this, this research set out to identify the relationship between compressive stress and the migration of GBM cells. This focus was chosen based on previous research that found other types of cancer cells have an invasive phenotype under compressive stress. Additionally, this research set out to identify the effects of physical forces induced by GBM within the brain, such as midline-shifts, on the behavior of GBM cells.

In this research, two GBM cell lines were studied, and it was found for both cell lines that increasing compressive stress increased the migration to a stress point, 23 Pa. After this point, compressive stress caused a decrease in migration. The U251 cell line had the slowest migration at this point of 23 Pa, probably because of its lower migration rate observed under normal conditions. This led to a less drastic bell curve compared to

LN229 cells lines, when observing the results of the compressive stress on migration speed.

Compressive stress caused the cells to decrease in area and ferret length at the peak migration compression, 23 Pa, when compared to normal conditions. However, for the U251 cell line, higher compressive stress led to the cell area and ferret length to increase. This decrease in area contradicts the previous study completed by Jain, in which they suggested that the increase in compressive stress increases the migration since the compressive stress flattens out the cells and pushes them towards migration. If this had been the case, there would have been an increase in cell area for the compressive stress. Therefore, to understand what is occurring, Western blots are being completed to study possible signaling pathways that may be causing this increase in migration under stress.

In addition to employing a 1D wound healing assay to evaluate migration, it was desired explore migration of cells under compression in environments with their accustomed biophysical properties. To do this, engineering a hydrogel with the same biophysical properties of the brain was necessary. This research is still in progress. Once completed, we will evaluate 3D single cell migration for all three cell lines. We expect these results to validate our findings that compressive stress causes a distribution of increasing migration at a specific peak, but then causes a decrease in migration at higher compressions. This peak point causing an increase in migration could possibly be due to the compression causing the cells to be under stress, reducing the actin that is attached,

causing their area to decrease, and increasing migration. However, further research into this mechanism must be explored.

References

[1] "Glioblastoma Multiforme." *American Association of Neurological Surgeons*. AANS, Oct. 2015. Web. 21 Aug. 2016.

[2] Tse, J.M., et al., *Mechanical compression drives cancer cells toward invasive phenotype.* Proceedings of the National Academy of Sciences of the United States of America, 2012. **109**(3): p. 911-6.

[3] "Glioblastoma (GBM)." Brain Tumor Symptoms, Treatment, Support, Research. American Brain Tumor Association, 2014. Web. 30 Aug. 2016.

[4] Stylianopoulos, T., et al., Causes, consequences, and remedies for growth-induced solid stress in murine and human tumors. Proceedings of the National Academy of Sciences of the United States of America, 2012. 109(38): p. 15101-8.

[5] Geer, C.P. and S.A. Grossman, Interstitial fluid flow along white matter tracts: A potentially important mechanism for the dissemination of primary brain tumors. Journal of Neuro-Oncology, 1997. 32(3): p. 193-201.

[6] Tse, J.M., et al., Mechanical compression drives cancer cells toward invasive phenotype. Proceedings of the National Academy of Sciences of the United States of America, 2012. 109(3): p. 911-6.

[7] (01.2014), Life Technolgies. Click-iT® Plus EdU Imaging Kits (Pub. No. MAN0009885 Rev. A.0) (n.d.): n. pag. Thermo Fisher. Thermo Fisher, 6 Jan. 2014. Web. 1 Apr. 2017.

[8] Mitra, S. K., Hanson, D. A., & Schlaepfer, D. D. (January 01, 2005). Focal adhesion kinase: in command and control of cell motility. Nature Reviews. Molecular Cell Biology, 6, 1, 56-68.

[9] Xie, Yuan, Tobias Bergström, Yiwen Jiang, Patrik Johansson, Voichita D. Marinescu, Nanna Lindberg, Anna Segerman, Grzegorz Wicher, Mia Niklasson, Sathishkumar Baskaran, Smitha Sreedharan, Isabelle Everlien, Marianne Kastemar, Annika Hermansson, Lioudmila Elfineh, Sylwia Libard, Eric C. Holland, Göran Hesselager, Irina Alafuzoff, Bengt Westermark, Sven Nelander, Karin Forsberg-Nilsson, and Lene Uhrbom. "The Human Glioblastoma Cell Culture Resource: Validated Cell Models Representing All Molecular Subtypes." Ebiomedicine. 2.10 (2015): 1351-1363. Print.

[10] Qi, Songtao, and Yawei Liu. "Differences in Protein Expression between the U251 and U87 Cell Lines." Turkish Neurosurgery (2016): n. pag. Web. 15 Apr. 2017.

[11] Beadle, C, MC Assanah, P Monzo, R Vallee, SS Rosenfeld, and P Canoll. "The Role of Myosin Ii in Glioma Invasion of the Brain." Molecular Biology of the Cell. 19.8 (2008): 3357-68. Print.

[13] Gomez-Roman, Natividad, Katrina Stevenson, Lesley Gilmour, Graham Hamilton, and Anthony J. Chalmers. "A Novel 3d Human Glioblastoma Cell Culture System for Modeling Drug and Radiation Responses." Neuro-oncology. (2016). Print.

Appendix A: Specific Aim 1 Raw Data

Table 3: LN229 Single Cell Migration Raw Data

Sample	Ln229_1		
time (hr)	18	time(s)	64800
Cell Number	Velocity	Length (um)	D2S
1	0.00086332	55.943	4.885
2	0.0011807	76.512	27.291
3	0.0012306	79.741	28.655
4	0.00088526	57.365	10.527
5	0.00089122	57.751	15.556
Sample	Ln229_2		
time (hr)	18	time(s)	64800
Cell Number	Velocity (um/s)	Length (um)	D2S
1	0.001078164	69.865	24.232
Sample	Ln229_3		
time (hr)	18	time(s)	64800
Cell Number	Velocity (um/s)	Length (um)	D2S
1	0.000372145	24.115	1.422
2	0.000834954	54.105	17.158
Sample	Ln229_4		
time (hr)	18	time(s)	64800
Cell Number	Velocity (um/s)	Length (um)	D2S
1	0.00080838	52.383	19.761
2	0.001211852	78.528	45.08
3	0.001177608	76.309	8.361

Table 4: U87 Single Cell Migration Raw Data

Sample	U87_1		
time (hr)	18	time(s)	64800
Cell Number	Velocity	Length (um)	D2S
1	0.001458256	94.495	10.676
2	0.000236497	15.325	10.126
3	0.000217716	14.108	12.116
4	0.000198935	12.891	12.655
5	0.000240818	15.605	7.707
Sample	U87_2		
time (hr)	18	time(s)	64800
Cell Number	Velocity	Length (um)	D2S
1	0.000570633	36.977	1.897
2	0.001121559	72.677	30.51
3	0.000941327	60.998	2.683
Sample	U87_3		
time (hr)	18	time(s)	64800
Cell Number	Velocity	Length (um)	D2S
1	0.000954367	61.843	9.349
2	0.001564105	101.354	13.219
3	0.000898904	58.249	12.374
Sample	U87_4		
time (hr)	18	time(s)	64800
Cell Number	Velocity	Length (um)	D2S
1	0.001109799	71.915	21.371
2	0.001287593	83.436	31.456
Sample	U87_5		
time (hr)	18	time(s)	64800
Cell Number	Velocity	Length (um)	D2S
1	0.001919707	124.397	33.66
2	0.000830262	53.801	8.008
3	0.001552809	100.622	19.871
4	0.000880725	57.071	2.452
Sample	U87_6		
time (hr)	18	time(s)	64800
Cell Number	Velocity	Length (um)	D2S

Table 4 Continued:

1	0.002158596	139.877	25.347
2	0.002291312	148.477	10.362
3	0.002740448	177.581	34.977
Sample	U87_7		
time (hr)	18	time(s)	64800
Cell Number	Velocity	Length (um)	D2S
1	0.00175267	113.573	19.337
2	0.000761343	49.335	23.915
3	0.002384892	154.541	23.558
4	0.002134676	138.327	26.91
Sample	U87_8		
time (hr)	18	time(s)	64800
Cell Number	Velocity	Length (um)	D2S
1	0.001588565	102.939	74.178
2	0.000659799	42.755	8.53
3	0.001501003	97.265	27.535
Sample	U87_9		
time (hr)	18	time(s)	64800
Cell Number	Velocity	Length (um)	D2S
1	0.000992886	64.339	13.039
2	0.001278796	82.866	42.122
3	0.001433735	92.906	5.551
Sample	U87_10		
time (hr)	18	time(s)	64800
Cell Number	Velocity	Length (um)	D2S
1	0.001928673	124.978	6.252
2	0.002471373	160.145	19.386
Sample	U87_11		
time (hr)	18	time(s)	64800
Cell Number	Velocity	Length (um)	D2S
1	0.001577284	102.208	26.19
2	0.00061537	39.876	11.023
3	0.000456528	29.583	3.396
4	0.001940988	125.776	26.083
5	0.000976173	63.256	0.993

Table 4 Continued:

Sample	U87_12		
time (hr)	18	time(s)	64800
Cell Number	Velocity	Length (um)	D2S
1	0.001188981	77.046	27.218
2	0.001732577	112.271	8.622
Sample	U87_13		
time (hr)	18	time(s)	64800
Cell Number	Velocity	Length (um)	D2S
1	0.001681975	108.992	65.818
2	0.002940355	190.535	13.589
3	0.002253086	146	65.032
4	0.001422886	92.203	24.709
Sample	U87_14		
time (hr)	18	time(s)	64800
Cell Number	Velocity	Length (um)	D2S
1	0.003131528	202.923	72.402
2	0.000803364	52.058	0.801
Sample	U87_15		
time (hr)	18	time(s)	64800
Cell Number	Velocity	Length (um)	D2S
1	0.00186034	120.55	50.141
2	0.001364707	88.433	12.567
3	0.001855123	120.212	5.277
4	0.000483627	31.339	1.884

Table 5: U251 Single Cell Migration Raw Data

Sample	U251_1		
time (hr)	18	time(s)	64800
Cell Number	Velocity	Length (um)	D2S
1	0.000863827	55.976	12.453
2	0.000548441	35.539	1.831
3	0.000843935	54.687	34.9
4	0.000797747	51.694	5.978

Table 5 Continued:

5	0.000847485	54.917	14.669
6	0.000609043	39.466	2.22
7	0.000750417	48.627	13.989
8	0.00036412	23.595	0.702
9	0.000191343	12.399	0.22
10	0.000549877	35.632	1.404
Sample	U251_2		
time (hr)	18	time(s)	64800
Cell Number	Velocity	Length (um)	D2S
1	0.000372423	24.133	1.256
2	0.00105838	68.583	0.993
3	0.001014722	65.754	1.57
Sample	U251_3		
time (hr)	18	time(s)	64800
Cell Number	Velocity	Length (um)	D2S
1	0.000457284	29.632	0.666
2	0.000510262	33.065	2.746
3	0.000732361	47.457	7.755
4	0.000456157	29.559	4.171
5	0.000430401	27.89	1.554
6	0.00048713	31.566	3.781
Sample	U251_4		
time (hr)	18	time(s)	64800
Cell Number	Velocity	Length (um)	D2S
1	0.000439877	28.504	2.531
2	0.000205	13.284	0.496
3	0.000667623	43.262	0.801
4	0.001074012	69.596	6.712
Sample	U251_5		
time (hr)	18	time(s)	64800
Cell Number	Velocity	Length (um)	D2S
1	0.000331142	21.458	2.71
2	0.001899707	123.101	5.79
3	0.000438796	28.434	1.11

Table 5 Continued:

4	0.00067716	43.88	5.59
5	0.000468148	30.336	4.577
Sample	U251_6		
time (hr)	18	time(s)	64800
Cell Number	Velocity	Length (um)	D2S
1	0.000255123	16.532	1.11
2	0.000461914	29.932	2.482
3	0.000865123	56.06	4.684
4	0.000508966	32.981	4.13
5	0.000703256	45.571	1.351
6	0.000370278	23.994	0.444
7	0.000967207	62.675	3.675
8	0.000741389	48.042	4.094
Sample	U251_7		
time (hr)	18	time(s)	64800
Cell Number	Velocity	Length (um)	D2S
1	0.00175267	113.573	19.337
2	0.000411219	26.647	23.915
3	0.000270864	17.552	23.558
4	0.0003125	20.25	26.91
Sample	U251_8		
time (hr)	18	time(s)	64800
Cell Number	Velocity	Length (um)	D2S
1	0.001906497	123.541	74.178
2	0.000659799	42.755	8.53
3	0.001459136	94.552	27.535
Sample	U251_9		
time (hr)	18	time(s)	64800
Cell Number	Velocity	Length (um)	D2S
1	0.000992886	64.339	13.039
2	0.001289475	83.558	42.122
3	0.001647269	106.743	5.551
Sample	U251_10		
time (hr)	18	time(s)	64800

Table 5 Continued:

Cell Number	Velocity	Length (um)	D2S
1	0.001928673	124.978	6.252
2	0.002471373	160.145	19.386
Sample	U251_11		
time (hr)	18	time(s)	64800
Cell Number	Velocity	Length (um)	D2S
1	0.000976173	63.256	0.993
2	0.000456528	29.583	3.396
3	0.001577284	102.208	26.19
4	0.000589398	38.193	11.023
5	0.001801296	116.724	26.083
Sample	U251_12		
time (hr)	18	time(s)	64800
Cell Number	Velocity	Length (um)	D2S
1	0.000467454	30.291	1.295
2	0.000582515	37.747	3.179
Sample	U251_13		
time (hr)	18	time(s)	64800
Cell Number	Velocity	Length (um)	D2S
1	0.000597022	38.687	7.259
2	0.00080446	52.129	2.482
3	0.000467438	30.29	1.295
4	0.000494707	32.057	1.422
5	0.000567608	36.781	0.702
Sample	U251_14		
time (hr)	18	time(s)	64800
Cell Number	Velocity	Length (um)	D2S
1	0.001219182	79.003	5.811
2	0.000839182	54.379	11.462
3	0.000472932	30.646	3.794
4	0.000359398	23.289	2.047
5	0.00041375	26.811	0.496
Sample	U251_15		
time (hr)	18	time(s)	64800

Table 5 Continued:

Cell Number	Velocity	Length (um)	D2S
1	0.000462222	29.952	1.79
2	0.001407654	91.216	3.14

Table 6: U87 (Edu Test) Proliferation Characterization Raw Data

Date	9/27/16	Sample #	1	
FITC	Number of Cells	DAPI	Number of Cells	FITC:DAPI
1	6	1	19	0.315789474
2	9	2	14	0.642857143
3	4	3	15	0.266666667
4	12	4	16	0.75
5	14	5	22	0.636363636
6	6	6	13	0.461538462
7	6	7	11	0.545454545
8	8	8	13	0.615384615
9	3	9	12	0.25
10	16	10	18	0.888888889
			Average	0.537294343
Date	10/27/16	Sample #	1	
FITC	Number of Cells	DAPI	Number of Cells	FITC:DAPI
1	25	1	66	0.378787879
2	30	2	86	0.348837209
3	8	3	16	0.5
4	10	4	28	0.357142857
5	15	5	31	0.483870968
6	24	6	64	0.375
7	14	7	46	0.304347826
8	8	8	34	0.235294118
9	20	9	45	0.444444444
10	15	10	33	0.454545455
			Average	0.388227076
Date	10/27/16	Sample #	2	

Table 6 Continued:

FITC	Number of Cells	DAPI	Number of Cells	FITC:DAPI
1	11	1	32	0.34375
2	24	2	73	0.328767123
3	40	3	105	0.380952381
4	27	4	74	0.364864865
5	4	5	5	0.8
6	5	6	9	0.555555556
7	3	7	12	0.25
8	20	8	21	0.952380952
9	5	9	14	0.357142857
10	24	10	63	0.380952381
			Average	0.471436612
Date	1/13/17	Sample #	1	
FITC	Number of Cells	DAPI	Number of Cells	FITC:DAPI
1	28	1	92	0.304347826
2	22	2	87	0.252873563
3	17	3	73	0.232876712
4	25	4	85	0.294117647
5	17	5	70	0.242857143
6	16	6	53	0.301886792
7	13	7	50	0.26
8	22	8	60	0.366666667
9	13	9	40	0.325
10	17	10	71	0.23943662
			Average	0.282006297
Date	1/13/17	Sample #	2	
FITC	Number of Cells	DAPI	Number of Cells	FITC:DAPI
1	19	1	68	0.279411765
2	20	2	76	0.263157895
3	17	3	61	0.278688525
4	14	4	79	0.17721519
5	25	5	69	0.362318841
6	18	6	66	0.272727273
7	11	7	51	0.215686275

Table 6 Continued:

8	21	8	53	0.396226415
9	19	9	68	0.279411765
10	13	10	58	0.224137931
			Average	0.274898187

Table 7: U251 (Edu Test) Proliferation Characterization Raw Data

Date	10/27/16	Sample #	1	
FITC	Number of Cells	DAPI	Number of Cells	FITC:DAPI
1	10	1	70	0.142857143
2	5	2	39	0.128205128
3	3	3	7	0.428571429
4	9	4	71	0.126760563
5	4	5	36	0.111111111
6	5	6	25	0.2
7	10	7	88	0.113636364
8	7	8	51	0.137254902
9	10	9	76	0.131578947
10	10	10	27	0.37037037
			Average	0.189034596
Date	10/27/16	Sample #	2	
FITC	Number of Cells	DAPI	Number of Cells	FITC:DAPI
1	9	1	66	0.136363636
2	5	2	40	0.125
3	5	3	83	0.060240964
4	14	4	111	0.126126126
5	10	5	70	0.142857143
6	1	6	3	0.333333333
7	2	7	5	0.4
8	6	8	60	0.1
9	4	9	63	0.063492063
10	11	10	51	0.215686275
			Average	0.170309954
These cells were determined to be sick so new cells started with low passage number				

Table 7 Continued:

Date	11/18/16	Sample #	1	
FITC	Number of Cells	DAPI	Number of Cells	FITC:DAPI
1	5	1	29	0.172413793
2	13	2	49	0.265306122
3	20	3	56	0.357142857
4	13	4	45	0.288888889
5	13	5	32	0.40625
6	11	6	29	0.379310345
7	18	7	49	0.367346939
8	16	8	61	0.262295082
9	9	9	35	0.257142857
10	13	10	40	0.325
11	11	11	39	0.282051282
			Average	0.305740742
Date	11/18/16	Sample #	2	
FITC	Number of Cells	DAPI	Number of Cells	FITC:DAPI
1	10	1	23	0.434782609
2	10	2	32	0.3125
3	6	3	38	0.157894737
4	11	4	31	0.35483871
5	9	5	45	0.2
6	9	6	43	0.209302326
7	4	7	12	0.333333333
8	11	8	34	0.323529412
9	13	9	50	0.26
10	19	10	50	0.38
			Average	0.296618113
Date	12/14/16	Sample #	1	
FITC	Number of Cells	DAPI	Number of Cells	FITC:DAPI
1	5	1	12	0.416666667
2	5	2	13	0.384615385
3	3	3	12	0.25
4	4	4	7	0.571428571
5	5	5	10	0.5
6	2	6	13	0.153846154

Table 7 Continued:

7	1	7	7	0.142857143
8	1	8	2	0.5
9	3	9	10	0.3
10	4	10	10	0.4
			Average	0.361941392

Table 8: LN229 (Edu Test) Proliferation Characterization Raw Data

Date	10/27/16	Sample #	1	
FITC	Number of Cells	DAPI	Number of Cells	FITC:DAPI
1	22	1	45	0.488888889
2	37	2	55	0.672727273
3	26	3	44	0.590909091
4	33	4	51	0.647058824
5	17	5	38	0.447368421
6	23	6	38	0.605263158
7	4	7	6	0.666666667
8	5	8	5	1
9	4	9	9	0.444444444
10	26	10	40	0.65
			Average	0.621332677
Date	10/27/16	Sample #	2	
FITC	Number of Cells	DAPI	Number of Cells	FITC:DAPI
1	25	1	41	0.609756098
2	17	2	27	0.62962963
3	18	3	28	0.642857143
4	9	4	18	0.5
5	6	5	7	0.857142857
6	18	6	31	0.580645161
7	22	7	29	0.75862069
8	21	8	30	0.7
9	14	9	21	0.666666667
10	17	10	32	0.53125
			Average	0.647656824

Appendix B: Specific Aim 2 Raw Data

Table 9: LN229 Wound Healing Assay Raw Data

Sample	**LN229**	**Date**	**1/17/17**
Condition	Area	WHA	
Control_initial	62214	0.253479924	
Control_Final	46444		
Agar_initial	71936	0.343388568	
Agar_Final	47234		
58Pa_initial	44585	0.259885612	
58Pa_final	32998		
114Pa_initial	73850	0.132335816	
114Pa_final	64077		
Sample	**LN229**	**Date**	**1/23/17**
Condition	Area	WHA	
Control_initial	80568	0.722880052	
Control_Final	22327		
Agar_initial	65147	0.741783965	
Agar_Final	16822		
58Pa_initial	2568.32	0.356154996	
58Pa_final	1653.6		
114Pa_initial	56910	0.241802847	
114Pa_final	43149		
165Pa_initial	40419	-0.074667854	
165Pa_final	43437		
Sample	**LN229**	**Date**	**2/21/17**
Condition	Area	WHA	
Control_initial	79680	0.473945783	
Control_Final	41916		
Agar_initial	68062	0.35545532	
Agar_Final	43869		
11Pa_initial	68402	0.684526768	
11Pa_final	21579		
23Pa_initial_1	57449	0.830806454	

23Pa_final_1	9720		

Table 9 Continued:

23Pa_initial_2	62978	0.67177427	
23Pa_final_2	20671		
47Pa_initial	67931	0.717507471	
47Pa_final	19190		
Sample	**LN229**	**Date**	**3/02/17**
Sample	Area	WHA	
Control_initial	82810	0.616737109	
Control_Final	31738		
Agar_initial	79971	0.295819735	
Agar_Final	56314		
11Pa_initial	57148	0.621019108	
11Pa_final	21658		
47Pa_initial	72491	0.534342194	
47Pa_final	33756		
Sample	**LN229**	**Date**	**3/4/17**
Sample	Area	WHA	
Control_initial	91731	0.568324776	
Control_Final	39598		
Sample	**LN229**	**Date**	**3/6/17**
Sample	Area	WHA	
Control_initial	66643	0.462974356	
Control_Final	35789		
Agar_initial	72810	0.418802362	
Agar_Final	42317		
11Pa_initial	63161	0.46501797	
11Pa_final	33790		
47Pa_initial	65461	0.5295825	
47Pa_final	30794		

Table 10: U251 Compressive Stress Wound Healing Assay Raw Data

Sample	U251	Date	2/6/17
Condition	Area	WHA	
Control_initial	3524.201	0.384742244	
Control_Final	2168.292		
11Pa_initial	3169.03	0.422418216	
11Pa_final	1830.374		
23Pa_initial	2922.161	0.522237139	
23Pa_final	1396.1		
Sample	U251	Date	2/12/17
Condition	Area	WHA	
Control_initial	68121	0.438190866	
Control_Final	38271		
Agar_initial	74953	0.398062786	
Agar_Final	45117		
23Pa_initial	65955	0.519414752	
23Pa_final	31697		
Sample	U251	Date	3/2/17
Condition	Area	WHA	
Control_initial	66990	0.372861621	
Control_Final	42012		
11Pa_initial	112585	0.540080828	
11Pa_final	51780		
23Pa_initial_1	69066	0.622998291	
23Pa_final_1	26038		
47Pa_initial	65497	0.599844268	
47Pa_final	26209		
Sample	U251	Date	3/4/17
Condition	Area	WHA	
Control_initial	92617	0.18364879	
Control_Final	75608		
Agar_initial	64320	0.330021766	

Table 10 Continued:

Agar_Final	43093		
23Pa_initial_1	68003	0.424069526	
23Pa_final_1	39165		
47Pa_initial	66977	0.383086731	
47Pa_final	41319		
Sample	U251	Date	3/6/17
Condition	Area	WHA	
Control_initial	82293	0.257883417	
Control_Final	61071		
Agar_initial	68673	0.368820352	
Agar_Final	43345		
11Pa_initial	63971	0.400196964	
11Pa_final	38370		
23Pa_initial_1	73679	0.45825812	
23Pa_final_1	39915		
47Pa_initial	62333	0.436109284	
47Pa_final	35149		

Table 11: LN229 Single Cell Morphology Data

LN229					
30617			30817		
Type	Average Area	Average Feret	Type	Average Area	Average Feret
Control_2	40.73107143	9.688642857	Control_6	34.54512	9.61896
Control_6	40.13333333	9.028666667	Control_4	37.27439474	9.533526316
Control_7	36.53783333	9.0931	Control_1	44.02722917	10.57414583
Agarcontrol_8	33.27785294	9.319058824	Agarcontrol_2	28.41793939	6.999575758
Agarcontrol_3	30.68047619	8.515595238	Agarcontrol_9	30.45586667	8.163
Agarcontrol_5	35.00895238	8.641714286	Agarcontrol_10	34.49473529	8.199205882
0.22g_10	24.78474359	8.098512821	0.22g_7	29.95975758	8.260272727
0.22g_4	26.43085106	8.31987234	0.22g_8	28.15189362	8.070446809
0.22g_8	21.62294828	7.725327586	0.22g_1	18.78976923	7.069246154
0.44g_9	25.96114706	7.910617647	0.44g_6	27.1735	7.421791667
0.44g_3	26.67662963	8.541888889	0.44g_2	25.42365517	7.129448276
0.44g_8	23.619125	7.02103125	0.44g_10	28.14012	8.06148
Average Control	39.13407937	9.270136508		38.6155813	9.908877383
Avg. Agar	32.98909384	8.825456116		31.12284712	7.787260547
Avg. 0.22g	24.27951431	8.047904249		25.63380681	7.799988563
Avg. 0.44g	25.41896723	7.824512595		26.91242506	7.537573314

Table 12: U251 Single Cell Morphology Data

U251					
30617			30817		
Sample	Average Area	Average Feret	Sample	Average Area	Average Feret
Control_1	29.66675	7.8795	Control_4	36.64260714	8.373214286
Control_2	16.1706	5.5426	Control_6	40.02436842	8.570052632
Control__4	17.627	5.94775	Control_7	39.27236364	9.197590909
Agarcontrol_7	49.14161538	9.960192308	Agarcontrol_3	30.66211111	7.807740741
Agarcontrol_8	51.16477778	11.44911111	Agarcontrol_8	43.00717647	10.27270588
Agarcontrol_6	40.1026	9.4618	Agarcontrol_2	21.03643478	7.665826087
0.22g_8	24.6932	8.006177778	0.22g_9	20.91515625	6.912
0.22g_7	23.13068182	7.404681818	0.22g_7	20.83371053	6.259078947
0.22g_2	23.90673585	8.557301887	0.22g_2	19.32864516	6.119354839
0.44g_3	54.8475	11.71694444	0.44g_8	50.39470833	11.41529167
0.44_7	25.628125	7.783178571	0.44g_3	37.83331818	10.06222727
0.44g_5	36.90964706	11.66335294	0.44g_2	33.6826875	9.2935
Average	21.15478333	6.456616667		38.6464464	8.713619275

Control					
Avg. Agar	46.80299772	10.29036781		31.56857412	8.582090903
Avg. 0.22g	23.91020589	7.989387161		20.35917065	6.430144595
Avg. 0.44g	39.12842402	10.38782532		40.63690467	10.25700631